Langmuir

ARTICLE

pubs.acs.org/Langmuir

Understanding the pH-Dependent Behavior of Graphene Oxide Aqueous Solutions: A Comparative Experimental and Molecular Dynamics Simulation Study

Chih-Jen Shih,[†,§] Shangchao Lin,[†,‡,§] Richa Sharma,[†] Michael S. Strano,[†] and Daniel Blankschtein*[,†]

[†]Department of Chemical Engineering and [‡]Department of Mechanical Engineering, Massachusetts Institute of Technology, Cambridge, Massachusetts 02139, United States

ABSTRACT: Understanding the pH-dependent behavior of graphene oxide (GO) aqueous solutions is important to the production of assembled GO or reduced GO films for electronic, optical, and biological applications. We have carried out a comparative experimental and molecular dynamics (MD) simulation study to uncover the mechanisms behind the aggregation and the surface activity of GO at different pH values. At low pH, the carboxyl groups are protonated such that the GO sheets become less hydrophilic and form aggregates. MD simulations further suggest that the aggregates exhibit a GO−water−GO sandwichlike structure and as a result are stable in water instead of precipitating. However, at high pH, the deprotonated carboxyl groups are very hydrophilic such that individual GO sheets prefer to dissolve in bulk water like a regular salt. The GO aggregates formed at low pH are found to be surface-active and do not exhibit characteristic features of surfactant micelles. Our findings suggest that GO does not behave like conventional surfactants in pH 1 and 14 aqueous solutions. The molecular-level understanding of the solution behavior of GO presented here can facilitate and improve the experimental techniques used to synthesize and sort large, uniform GO dispersions in a solution phase.

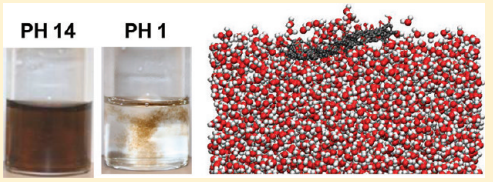

1. INTRODUCTION

In recent years, as an alternative approach to producing graphene on a large scale,[1−3] the exfoliation of graphite oxide has triggered considerable research efforts aimed at demonstrating its chemical and electronic properties.[4,5] The resulting thin graphene oxide (GO) sheets can be easily dispersed in an aqueous medium without adding amphiphilic stabilizers, including subsequently carrying out the necessary solution-phase chemistry. The oxygen-derived functional groups on the sheet basal plane and sheet edge allows GO to be reactive with organic and inorganic chemicals such that a rich variety of functional hybrids and complexes can be synthesized.[4,5] In addition, the molecular orbital change of sp^3 to sp^2 carbons through reduction chemistry can restore the graphene lattice to some extent.[6,7] Furthermore, the tunable conductivity and electronic band gap provide a controllable route to transforming an insulator to a graphenelike semimetal.[5] Because of these interesting GO properties, a broad spectrum of potential applications ranging from printable electronics and solar cells to biosensors have been proposed. To control the processes of exfoliation, dispersion, functionalization, and self-assembly[8] of the suspended GO sheets in aqueous media, a fundamental understanding of their solution behavior is in order.[4]

The chemical structure of GO is heterogeneous, and the coverage of oxygen groups varies depending on the degree of oxidation in the preparation processes.[4] To date, the most widely accepted structural model of GO is based on a series of analyses performed by Lerf and Klinowski.[9] These analyses indicated that the functional groups on the basal plane of the GO sheet consists primarily of hydroxyl and epoxy groups and that only small quantities of carboxyl groups are present at the edge of the GO sheets.[9] Considering the excellent ability of water to disperse GO, this material was initially assumed to be hydrophilic, with the hydrophilicity resulting from the hydroxyl and epoxy groups present in the GO sheet basal plane.[1] However, recent experiments involving pH changes and salt addition suggest that the peripheral carboxyl groups actually play a key role in determining the solution behavior of GO.[10] The colloidal stability of aqueous GO solutions has been attributed to the electrostatic repulsions between ionized carboxyl groups.[10] The pH-dependent hydrophilicity of GO has been exploited to control its assembly behavior using either the Langmuir−Blodgett (LB)[2,8] or the electrophoretic-deposition (EPD)[11] technique. Recently, Kim et al. further suggested that GO behaves like a surfactant, as determined by its ability to adsorb at a water−air interface, including lowering the surface tension of water.[8,12] In addition, GO has been used to stabilize Pickering emulsions of organic solvents,[12] polystyrene particles,[13] and carbon nanotube dispersions[12] in water. The basal plane of GO is much more hydrophobic than the carboxyl-decorated edges, and the large differences in both the hydrophilicity and structural dimensions make GO behave like an amphiphile. However, it is still very controversial to view GO as a conventional surfactant. Indeed, the most salient signature of surfactants in water—their ability to

Received: September 14, 2011
Revised: October 28, 2011
Published: October 31, 2011

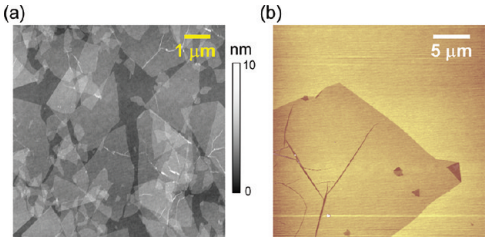

Figure 1. AFM images of (a) the synthesized GO sheets on a SiO_2 substrate and (b) a large GO sheet found on the same substrate.

micellize[14]—has not yet been reported for GO. Interestingly, very little is known about the fundamentals of GO aqueous solutions in terms of molecular details about the interactions between the functional groups and water molecules, including correlating these interactions with the observed pH-dependent surface activity and colloidal stability. Although a recent molecular dynamics (MD) simulation study[15] has shown that GO can form stable hydrogen-bonding networks with water molecules in a vapor phase, it did not consider the effects of the edge carboxyl groups, which, as discussed above, are critical to elucidating the pH-dependent behavior of GO in the bulk water phase.

With all of the above in mind, in this article we report on a series of comparative experimental and MD simulation studies that were carried out to understand the fundamentals of the surface activity and colloidal stability of GO aqueous solutions at different pH values. Specifically, we measured (i) the zeta potential, (ii) the colloidal size distribution, and (iii) the surface tension in acidic (pH 1) and basic (pH 14) GO aqueous solutions. In addition, the potential of mean force (PMF) between two parallel GO sheets in water and the free-energy change during the adsorption of a GO sheet from the bulk water phase to the water−vacuum interface were calculated using all-atomistic MD simulations. The results presented here provide fundamental, molecular-level insights into the pH-dependent behavior of GO aqueous solutions.

2. METHODS

2.1. Synthesis and Characterization. Graphite oxide was synthesized through the reaction of graphite powder (Bay Carbon SP-1) with potassium permanganate in a concentrated sulfuric acid solution (the Hummers method).[16,17] After oxidation, graphite oxide was dialyzed by suspending in deionized (DI) water to remove metal ions and acids. This solution was centrifuged to obtain concentrated graphite oxide as a precipitate. To obtain GO suspensions, the graphite oxide powder was exfoliated and dispersed in DI water by applying 5 min of bath sonication (with a Branson model 2510), and finally a stable, homogeneous, dark-brown solution was formed. The solution was stable and aged for approximately 2 years. The acidic (pH 1) and basic (pH 14) GO solutions were prepared using 1 M hydrogen chloride (HCl) and 2 M sodium hydroxide (NaOH) solutions as the source materials, respectively. The thickness of monolayer-exfoliated graphite oxide, GO, is around 1 nm. (See the AFM image in Figure 1a.) In addition, large GO flakes of up to 20 μm in size can be readily found (Figure 1b). All AFM images are topographic. Note that we also observed many multilayer/folded GO sheets after depositing the GO dispersions onto a substrate. However, it is difficult to tell whether the formation of these multilayer sheets is due to the reaggregation of GO during the deposition process or the originally unexfoliated GO sheets.

2.2. Zeta Potential and Particle Sizing. The zeta potential was measured using a Brookhaven ZETA PALS with irradiation from a 633 nm He−Ne laser. The samples were injected into capillary cells, and the electrophoretic mobility was estimated using a combination of electrophoresis and phase analysis light-scattering (PALS) techniques. The zeta potential, ζ, can be calculated from the electrophoretic mobility, η, using the Smoluchowski expression for platelike particles:[18] $\zeta = \eta\mu/\varepsilon$, where μ is the viscosity of water and ε is the dielectric permittivity of water. The same equipment was utilized to analyze the particle sizing of GO dispersions using the dynamic light scattering (DLS) technique at 90°. For each measurement, 10 runs with 20 cycles per run were carried out, and the values of the 5 final runs were averaged to yield the zeta potential and the particle size distribution for that measurement.

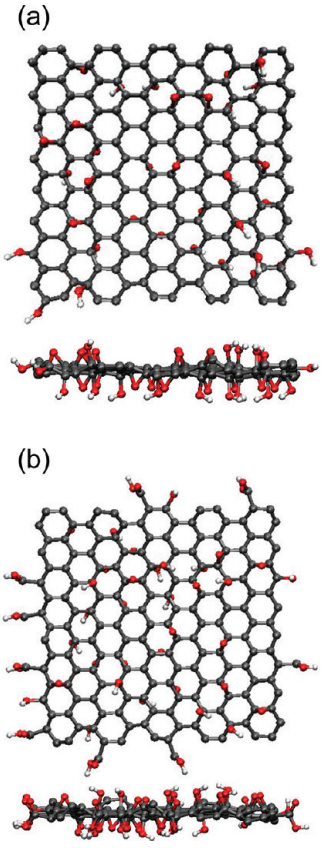

Figure 2. Top view (top) and side view (bottom) of the energy-minimized molecular structures of the GO sheets considered in this study: (a) $C_{10}O_1(OH)_1$ and (b) $C_{10}O_1(OH)_1(COOH)_{0.5}$. Each sphere represents an atom using the following color scheme: white, hydrogen; red, oxygen; and gray, carbon.

2.3. Surface Tension Measurements. A series of surface tension measurements were carried out as a function of GO concentration using a Krüss K100MK2 tensiometer. All measurements were carried out at room temperature. For each measurement, 20 surface tension readings were obtained, 3 s apart, and the final 10 readings were averaged to yield the surface tension for that measurement (with the first 10 measurements serving as an equilibration period). The surface tension variation for the last 10 readings was typically <0.3 mN/m. The concentration of GO was determined by the vacuum filtration technique. Two pieces of filter paper with a 1 μm pore size were used to collect GO dispersions during filtration. The highest concentration considered here is 1 mg/mL.

2.4. Molecular Dynamics Simulations. We carried out MD simulations to calculate the potential of mean force (PMF) between two parallel GO sheets as a function of the intersheet separation, d, and the

dx.doi.org/10.1021/la203607w |*Langmuir* 2012, 28, 235–241

free-energy change during adsorption by pulling a GO sheet from the bulk water phase ($z < 0$) to the water−vacuum interface ($z = 0$). Most simulations were carried out under the NPT ensemble (constant number of atoms, constant pressure of 1.0 bar, and constant temperature of 298.15 K), except for those involving water−vacuum interfaces, which were carried out under the NVT ensemble to generate a large vacuum space on top of the water phase in the simulation box. The optimized potentials for liquid simulations-all atoms (OPLS-AA)[19] force field implemented in the GROMACS 4.0[20] software package was used for all simulations. The water molecules were simulated using the standard SPC/E model.[21] The bond lengths for water molecules during simulations were constrained using the SETTLE algorithm.[22] Bond lengths in the solvent molecules were constrained using the parallel version of the LINCS algorithm.[23,24] van der Waals (vdW) interactions were treated with a cutoff distance of 0.9 nm.[25] Long-range electrostatic interactions were treated using the particle-mesh Ewald (PME) summation method.[26,27]

All of the sp^2 carbon atoms in GO were treated as uncharged Lennard-Jones (LJ) spheres using the force-field parameters reported by Tummala et al.[28] The force-field parameters for bonded interactions of unfunctionalized carbon atoms in graphene, including the bond stretching, angle, and dihedral potentials, were reported by Patra et al.[29] The epoxy and hydroxyl groups were randomly grafted to the carbon atoms on a 2.1 nm × 2.1 nm graphene basal plane (one of two surfaces). The carboxyl groups were also attached to the carbon atoms on the edge randomly. The GO model considered here is not significantly oxidized: $C_{10}O_1(OH)_1$ (i.e., 1 epoxy group and 1 hydroxyl group per 10 carbon atoms are attached to the graphene basal plane), as shown in Figure 2a. This GO model reflects a typical outcome of a standard oxidation process.[15] To model the pH effects, 1 carboxyl group per 20 carbon atoms was attached to the graphene edge ($C_{10}O_1(OH)_1(COOH)_{0.5}$), as shown in Figure 2b, and the edge carboxyl groups were either completely protonated ($C_{10}(O)_1(OH)_1(COOH)_{0.5}$) or completely deprotonated ($C_{10}(O)_1(OH)_1(COO^-)_{0.5}$) to mimic the behavior of GO in pH 1 or 14 solutions, respectively. To calculate the number of hydrogen bonds between GO and the surrounding water molecules, a geometrical criterion is used. Specifically, we consider a bond to be a hydrogen bond only if it meets the following two criteria: the donor−acceptor distance is smaller than 0.35 nm and the hydrogen donor−acceptor angle is larger than 30°.[20]

The equations of motion were integrated with a time step of 2 fs using the Verlet (leap-frog) algorithm.[30,31] The velocity-rescaled Berendsen thermostat was implemented to maintain the system at a constant temperature.[32] The pressure was coupled to an isotropic Berendsen barostat.[33] Periodic boundary conditions were applied in all three directions. The trajectories, velocities, and forces corresponding to all of the atoms in the system were saved every 10 000 steps (20 ps). Before carrying out the PMF calculations, the entire system was energy-minimized and the internal coordinates of the GO sheet were fixed. The PMF between two fixed parallel GO sheets was calculated by numerically integrating, using the trapezoidal method, the interaction forces required to separate the two GO sheets at various intersheet separations, d.[25,34] This integration process begins from the largest intersheet separation (20 Å), at which the PMF is set to be zero, and ends at the smallest intersheet separation simulated (6 Å). The choice of the largest and the smallest distances will be explained in the next section. The initial configurations were generated by placing two parallel graphene sheets at different intersheet separations, followed by filling the simulation box with sufficient randomized water molecules. Similarly, the free-energy change during adsorption was calculated by pulling the center of mass (COM) of a GO sheet from bulk water to the water−vacuum interface. The interaction forces required to keep the GO sheet at various distances from the water−vacuum interface were numerically integrated to yield the free-energy change during adsorption.[35]

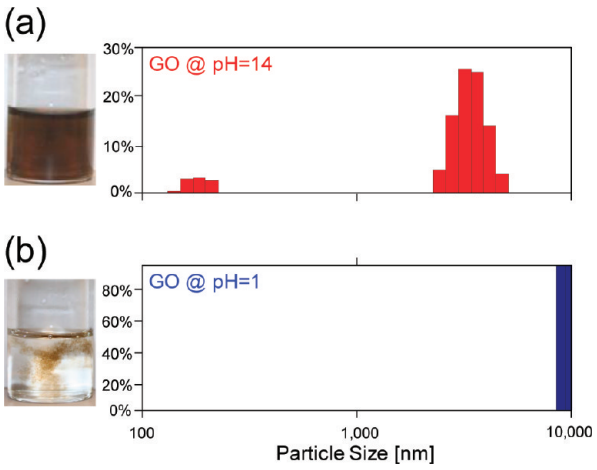

Figure 3. Photograph of a 1 mg/mL GO dispersion (left) and its colloidal size distribution (right) measured using the DLS technique at (a) pH 14 and (b) pH 1.

Note that the water−vacuum interface was located at $z = 0$ Å, where the z axis is normal to the interface. During the pulling process, the GO sheet is allowed to translate along the xy plane and to rotate around the COM. This integration process begins from the center of the water box ($z = -25$ Å), at which the free energy is set to be zero (the reference state), and ends at a distance far away from the water−vacuum interface ($z = 5$ Å) in vacuum. For each calculation, because the interaction forces take 1−3 ns to reach equilibrium, each simulated system was equilibrated for 10 ns and only the last 5 ns of simulation was used for data analysis.

3. RESULTS AND DISCUSSION

3.1. pH-Dependent Colloidal Stability. First, we discuss the role of the edge carboxyl groups in stabilizing GO sheets in water. To this end, the as-synthesized GO solutions (pH ∼5) were slightly diluted to 1 mg/mL with a concentrated HCl or NaOH solution to reach the desired pH values (1 and 14, respectively). At pH 14, the solution is visually homogeneous with a dark-brown color, as shown in the left image of Figure 3a. Note that these visual observations cannot provide detailed information about the solubility (or dispersity) of GO in the solution. However, the GO solution at pH 1 exhibits a very different appearance, as shown in the left image of Figure 3b. Large-scale visible aggregation occurs (the aggregates are millimeters in size) such that the GO solution becomes much more transparent because of the significant reduction in the number density of GO scattering centers. This pH-dependent aggregation has been utilized to modulate the hydrophilicity of assembled EPD films.[11] Interestingly, the aggregates do not settle down as a precipitate but instead remain dispersed and stable in the solution. This observation implies that the GO aggregates that form are complexes consisting of GO sheets and a large number of water molecules such that their mass density is similar to that of water.

The particle size distribution of suspended GO was also measured using dynamic light scattering (DLS) to understand the colloidal homogeneity of the solution better. It is noteworthy that the DLS measurement is based on the assumption that all particles are effective spheres and undergo Brownian motion in the solution. Because of the special geometrical structure of GO (a one-atom-thick sheet with a lateral size of micrometers), it

dx.doi.org/10.1021/la203607w |*Langmuir* 2012, 28, 235–241

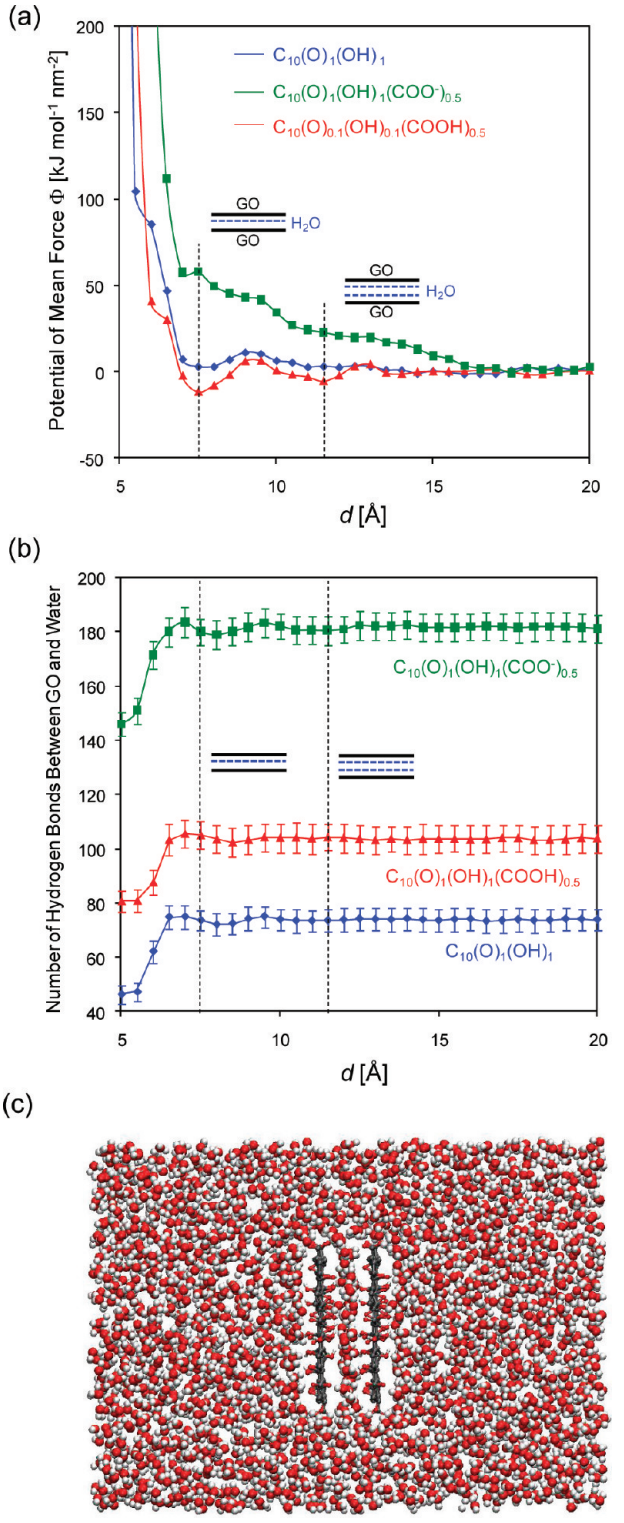

Figure 4. Simulated (a) potential of mean force between two parallel, fixed GO sheets and (b) the number of hydrogen bonds formed between the two sheets and the surrounding water molecules as a function of the intersheet separation, d. Three forms of GO $\{C_{10}(O)_1(OH)_1$, $C_{10}(O)_1(OH)_1(COOH)_{0.5}$, and $C_{10}(O)_1(OH)_1(COO-)_{0.5}\}$ are considered. The vertical dashed lines correspond to the energy-minimized configurations of GO/single-layer water/GO and GO/two-layer water/GO sandwich structures. (c) Postequilibrium MD simulation snapshot of two parallel $C_{10}O_1(OH)_1(COOH)_{0.5}$ sheets solvated in water at d = 7.5 Å showing a single layer of water molecules being confined between the two GO sheets. Color code: red, oxygen; white, hydrogen; and gray, carbon.

appears that the DLS technique is not quantitatively reliable. Therefore, the DLS analysis presented here should be viewed only as a qualitative indicator to shed light on the pH-dependent aggregation of GO. As shown on the right side of Figure 3a, at pH 14, two different sizes of particles with effective radii of around 200 nm and 3 μm are detected using DLS. The following mechanism leading to this size distribution may be invoked: the two observed sizes correspond to completely exfoliated (monolayer) GO and partially exfoliated (multilayer) GO (the thickness of GO affects the intensity of the scattered light).

However, at pH 1, the colloidal size detected is beyond the limit of the DLS technique (>10 μm) because of the aggregation of GO, as shown on the right of Figure 3b. In addition, the zeta potentials corresponding to the two solutions were measured and had values of -4.25 ± 0.35 and -44.73 ± 1.54 mV for the pH 1 and 14 GO solutions, respectively. The negative zeta potential values indicate that the surface charges are negative (COO^- groups) and depend on the degree of deprotonation of the edge carboxyl groups. The measured zeta potential values are consistent with the reported values.[10,11] The dramatic change in the zeta potential at pH 1 and 14 reflects the fact that the edge carboxyl groups are highly protonated at pH 1. As a result, the zeta potential of the charged GO surfaces becomes much less negative and leads to colloidal instability. These findings suggest that the electrostatic repulsions between ionized carboxyl groups at the GO sheet edges provide the major barrier preventing the GO sheets from aggregating.[10,11]

To understand further the pH-dependent aggregation of GO at the molecular level, MD simulations of two parallel GO sheets solvated in a 5 × 5 × 7 nm^3 water box were carried out to investigate the interactions of the GO sheets through water. Note that the size of the simulation box was chosen to eliminate interactions between the GO sheets and their periodic images. The potential of mean force (PMF) of GO per unit area per mole, Φ, was simulated as shown in Figure 4a. Three forms of GO $\{C_{10}(O)_1(OH)_1$, $C_{10}(O)_1(OH)_1(COOH)_{0.5}$, and $C_{10}(O)_1(OH)_1(COO^-)_{0.5}\}$ were considered. The time-averaged numbers of hydrogen bonds formed between the two GO sheets and the surrounding water molecules were also calculated as a function of d, as shown in Figure 4b. At large d values (d > 14 Å), for $C_{10}(O)_1(OH)_1$ and $C_{10}(O)_1(OH)_1(COOH)_{0.5}$, the two GO sheets cannot feel each other through the aqueous medium such that the interaction forces between them are close to zero (blue and red curves in Figure 4a). For d > 14 Å, the $C_{10}(O)_1(OH)_1$, $C_{10}(O)_1(OH)_1(COOH)_{0.5}$, and $C_{10}(O)_1(OH)_1(COO^-)_{0.5}$ sheets establish 75, 105, and 180 hydrogen bonds with the surrounding water molecules, respectively (Figure 4b). These differences result from different degrees of hydrophilicity among the three species. However, for $C_{10}(O)_1(OH)_1(COO^-)_{0.5}$ at d > 17 Å (green curve in Figure 4a), the long-range electrostatic repulsion is mostly screened by the water molecules confined between two GO sheets such that the interaction force is relatively weak. As d decreases (d < 17 Å), the PMF between two GO sheets increases gradually because of the electrostatic repulsions between the carboxyl groups on the two sheets (green curve in Figure 4a).

As d decreases further, the confined water molecules form two-layer (10 Å < d < 14 Å) and single-layer (6 Å < d < 10 Å) structures, finally resulting in a water-depleted region (d < 6 Å) (Figure 4b). The variation in the confined water layers between two GO sheets results in oscillatory interaction forces between the two sheets.[14,36] This in turn leads to the oscillations observed in the PMF and in the number of hydrogen bond curves for

dx.doi.org/10.1021/la203607w |Langmuir 2012, 28, 235–241

6 Å < d < 14 Å Figure 4a,b). The two minima in the PMF located at d = 7.5 and 11.5 Å (vertical dashed lines in Figure 4a) correspond to the energy-minimized configurations of GO/single-layer water/GO and GO/two-layer water/GO sandwich structures, as shown in the insets in Figure 4a. The simulated configuration with a single layer of water molecules confined between two $C_{10}(O)_1(OH)_1(COOH)_{0.5}$ sheets (at d = 7.5 Å) is shown in Figure 4c. For $C_{10}(O)_1(OH)_1(COOH)_{0.5}$, these two configurations exhibit −11.6 and −5.4 kJ mol^{-1} nm^{-2} of free-energy change compared to the reference state (a single GO sheet in bulk water). In addition, as shown in Figure 4b, the number of hydrogen bond curves show maxima at $d \approx 7$ Å, which is very close to the separation corresponding to the energy-minimized configuration of the GO/single-layer water/GO structure. The increase in the number of hydrogen bonds, which results from the confinement-induced ordering of the single-layer water molecules,[37] also assists in stabilizing this sandwich structure. In other words, the PMF curve indicates that the GO sheets with edge carboxyl groups at low pH ($C_{10}(O)_1(OH)_1(COOH)_{0.5}$) tend to aggregate and form GO/water/GO sandwichlike structures with surrounding water molecules. However, for $C_{10}(O)_1(OH)_1$, although the two minima exist, the corresponding free-energy changes are both positive (+2.9 and +3.0 kJ mol^{-1} nm^{-2}), as shown in Figure 4a. As d decreases, it appears that the formation of hydrogen-bonding networks around the protonated carboxyl groups is capable of stabilizing the GO/water/GO sandwichlike structure. Accordingly, it is quite clear that the protonated carboxyl groups at the GO edges can facilitate the aggregation of GO sheets through confined single- or two-layer water molecules. The molecular insight provided by the MD simulation results clearly explains the GO aggregation phenomena observed experimentally at pH 1. However, as shown in Figure 4a for $C_{10}(O)_1(OH)_1(COO^-)_{0.5}$, as d decreases (d < 17 Å), because the increase in the electrostatic repulsion becomes stronger, the local minima in the PMF associated with the one-layer and two-layer sandwichlike structures are not obvious. As we mentioned earlier, $C_{10}(O)_1(OH)_1(COO^-)_{0.5}$ forms many more hydrogen bonds with the surrounding water molecules because of its higher hydrophilicity (Figure 4b). The curve of the change in the number of hydrogen bonds shows a similar trend to those for $C_{10}(O)_1(OH)_1$ and $C_{10}(O)_1(OH)_1(COOH)_{0.5}$. Compared to its PMF profile, it appears that the increase in the number of hydrogen bonds is not enough to stabilize the sandwichlike structures. The strong electrostatic repulsions between the $C_{10}(O)_1(OH)_1(COO^-)_{0.5}$ sheets tend to exfoliate and stabilize them in water, as we observed experimentally (Figure 3a). Our analysis also suggests an interesting new strategy for preparing ultralarge GO sheets in a solution phase:[38] exfoliating graphite oxide in high-pH aqueous media.

For d < 6 Å, the dramatic increase in the interaction potential between GO and the water molecules destabilizes the single layer of water molecules, which in turn leads to the desorption of the confined water molecules.[25] This behavior is related to the steric hindrance discussed by Choudhury and Pettitt.[39] Because no water molecules reside between the two GO sheets for d < 6 Å, the intersheet vdW interaction potential dominates and the repulsive interactions between the functional groups on GO increase the intersheet PMF dramatically, as shown in Figure 4a. However, as shown in Figure 4b, the sudden decrease in the number of hydrogen bonds for d < 6 Å clearly results from the depletion of confined water molecules between two GO sheets.

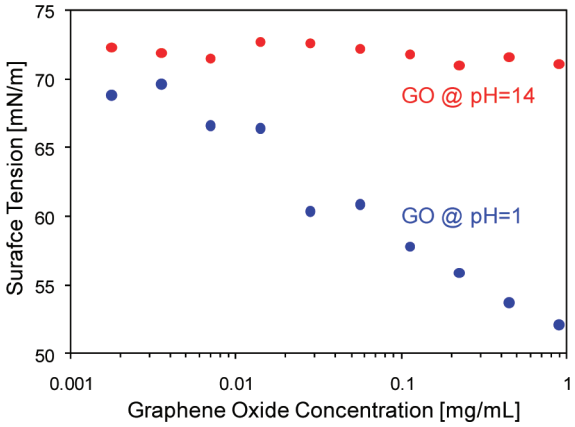

Figure 5. Experimentally measured surface tension as a function of GO concentration at pH 14 (red dots) and pH 1 (blue dots).

3.2. pH-Dependent Surface Activity. As discussed in section 3.1, the edge carboxyl groups on GO sheets at different pH values can be simply viewed as a tunable means to change the hydrophilicity of GO in aqueous media. Although it has recently been suggested that GO behaves like a surfactant in aqueous media because of the difference in hydrophilicity between the edge and the basal plane,[12] one of the most salient properties of conventional surfactants (i.e., their ability to micellize) has not been investigated. Recall that conventional surfactant monomers reduce the surface tension of water by adsorbing at the water−air interface at low concentration and assemble into micelles when the surfactant concentration exceeds the critical micelle concentration (cmc). Because it is thermodynamically more favorable for the surfactant monomers to form micelles in the bulk aqueous phase rather than to adsorb at the surface above the cmc, the surface tension shows a much weaker concentration dependence at surfactant concentrations that exceed the cmc.[14]

With the above brief background on surfactant micellization in mind, to understand further the pH effects on the surface activity of GO, the surface tension of water was measured as a function of GO concentration at pH 1 and 14 (Figure 5). Because of the deprotonation of the edge carboxyl groups, the difference in the degrees of hydrophilicity between the edge and the basal plane is maximized at pH 14 and minimized at pH 1. In other words, GO may be expected to behave more like a surfactant at high pH. However, as Figure 5 reveals, the measured surface tension of GO at pH 14 is around 72 dyn/cm and shows a very weak dependence on the GO concentration. In fact, the measured surface tension values at pH 1 are all very close to that of pure water (72.8 dyn/cm). Accordingly, GO at pH 14 in not surface-active and dissolves in water like a regular salt, in spite of the fact that it is expected to behave more like a surfactant. On the basis of the surface tension results, at pH 14 it appears that the deprotonated edge carboxyl groups are able to pull the entire GO sheet into the bulk water phase, although it possesses a relatively hydrophobic basal plane. In addition, as discussed in section 3.2, the GO sheets at high pH do not micellize in bulk water because the electrostatic repulsions between the carboxyl groups hinder GO aggregation.

In the case of GO at pH 1, the surface tension decreases gradually from ∼70 to ∼52 dyn/cm as the GO concentration increases (Figure 5). Therefore, it appears that the GO sheets at pH 1 are surface-active. Interestingly, the surface tension does

dx.doi.org/10.1021/la203607w |*Langmuir* 2012, 28, 235–241

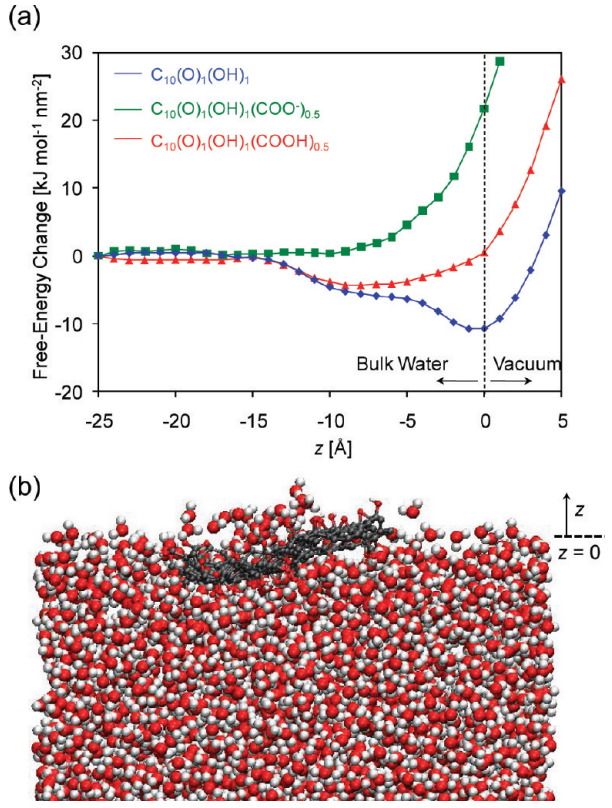

Figure 6. (a) Simulated free-energy change during adsorption from bulk water to the water−vacuum interface as a function of the distance from the interface, z, for the three forms of GO considered. (b) Postequilibrium MD simulation snapshot of a $C_{10}O_1(OH)_1$ sheet adsorbed at the water−vacuum interface (located at $z = 0$). Color code: red, oxygen; white, hydrogen; and gray, carbon.

not reach a plateau at this GO concentration but instead continues to decrease gradually (Figure 5). At the highest GO concentration considered (1 mg/mL, section 2), the surface tension still does not yet reach a plateau. Our findings suggest that the aggregation of the GO sheets at low pH cannot be viewed as conventional micellization. In addition, we have shown that the aggregation of the GO sheets at pH 1 can be visually observed when the GO concentration exceeds 0.01 mg/mL (section 3.1). Therefore, the GO aggregates at pH 1 are non-micelle-like and tend to adsorb to the water−air interface instead of staying in the bulk aqueous phase. This is due to the fact that the area of the GO basal plane is so large that the assembled GO structure is still too hydrophobic. Considering its low mass density due to the GO/water/GO sandwichlike structures formed (section 3.1), it is not surprising that the GO aggregates that form can rise and adsorb at the water−air interface. Therefore, we conclude that, with respect to micellization, GO does not behave like a conventional surfactant at either pH value, although it is surface-active at pH 1.

To substantiate these interesting findings, MD simulations were carried out to understand better the surface activity of GO on the molecular level. For this purpose, one sheet of GO (area = 21 × 21 Å^2) was first solvated in the center of a 5 × 5 × 5 nm^3 water box as a subsystem; subsequently, two additional vacuum spaces were added to the top and the bottom of the subsystem along the z axis. Therefore, an overall 5 × 5 × 15 nm^3 simulation cell was considered, with the water subsystem positioned in the middle. The simulation box was chosen to eliminate the interactions between the GO sheet and its periodic images. The free-energy change during the adsorption of a GO sheet from bulk water to a water−vacuum interface per unit area per mole of GO was calculated by integrating the interaction force between the GO sheet and the water molecules as a function of the z coordinate[35] (Figure 6a). For the three forms of GO considered, the interactions are weak for $z < -15$ Å, where the GO sheets cannot feel the presence of the water−vacuum interface. The main reason for this result is that the dimension of a GO sheet considered here is 21 Å, with the GO sheet being able to rotate freely as well as to translate parallel to the interface (any x and y values) during the center-of-mass (COM) pulling process. As a result, the distance between the COM of GO and the water−vacuum interface (15 Å) is about half of the diagonal size of the GO sheet. As z increases, the three forms of GO behave differently depending on their degrees of hydrophilicity. For example, $C_{10}(O)_1(OH)_1(COO^-)_{0.5}$ is the most hydrophilic form (Figure 4b); therefore, the free-energy change during adsorption to the water−vacuum interface increases continuously as a function of z (green curve in Figure 6a). As Figure 6a reveals, a +22 kJ mol^{-1}nm^{-2} free-energy change is required to pull a single sheet of $C_{10}(O)_1(OH)_1(COO^-)_{0.5}$ from bulk water to the interface located at $z = 0$. It appears that $C_{10}(O)_1(OH)_1(COO^-)_{0.5}$ is not surface-active. However, for the two less hydrophilic forms of GO {$C_{10}(O)_1(OH)_1(COOH)_{0.5}$ (red curve in Figure 6a) and $C_{10}(O)_1(OH)_1$ (blue curve in Figure 6a)}, both free-energy curves show a minimum near the water−vacuum interface. Note that in the case of $C_{10}(O)_1(OH)_1(COOH)_{0.5}$ the location of the minimum at $z = -8$ Å results from an asymmetric distribution of carboxyl groups to the four edges of GO. (The edge carboxyl groups were attached to the edge carbons randomly). At least −5 kJ mol^{-1} nm^{-2} (at $z = -8$ Å) and −11 kJ mol^{-1} nm^{-2} (at $z = 0$ Å) free-energy changes are needed to pull a $C_{10}(O)_1(OH)_1(COOH)_{0.5}$ and a $C_{10}(O)_1(OH)_1$ sheet close to the interface, respectively. This, in turn, indicates that the adsorption process is thermodynamically favorable and spontaneous. Both $C_{10}(O)_1(OH)_1(COOH)_{0.5}$ and $C_{10}(O)_1(OH)_1$ are surface-active. Figure 6b shows the MD simulated configuration of a $C_{10}(O)_1(OH)_1$ sheet corresponding to the minimum in its free-energy curve at $z = 0$, adsorbed at the water−vacuum interface. To minimize its contact area with the surrounding water molecules, the $C_{10}(O)_1(OH)_1$ sheet tends to be parallel to the interface. From a practical viewpoint, because $C_{10}(O)_1(OH)_1$ can be regarded experimentally as a very large GO sheet (the effect of the edge carboxyl groups is negligible),[12] the size sorting of GO dispersions using the CO_2 floatation technique[8,12] should be carried out at high pH such that all of the smaller GO sheets may be retained in the bulk aqueous phase.

4. CONCLUSIONS

A comparative study that combines experiments and MD simulations was carried out to understand the effects of pH on the colloidal stability and surface activity of GO aqueous solutions. Three GO models {$C_{10}(O)_1(OH)_1$, $C_{10}(O)_1(OH)_1(COOH)_{0.5}$, and $C_{10}(O)_1(OH)_1(COO^-)_{0.5}$} were considered in the MD simulations. The reported pH-dependent behavior originates from the degree of deprotonation of the carboxyl groups at the edges of GO sheets. The electrostatic repulsions between the ionized carboxyl groups are the major driving force

for the observed dissolution of individual GO sheets at higher pH. At low pH, the carboxyl groups are protonated such that the GO sheets become less hydrophilic and form suspended GO aggregates. As confirmed by the PMF calculations, the aggregates are GO/water/GO sandwichlike structures and can be suspended in a stable manner in water instead of settling down. On the basis of these analyses, we suggest that the exfoliation of graphite oxide should be carried out in a base solution to enlarge the size of the dispersed GO.

A series of surface tension measurements further suggest that GO does not behave like a conventional surfactant in pH 1 and 14 aqueous solutions. At higher pH, the carboxyl groups are deprotonated and the difference in the degree of hydrophilicity between the edge and the basal plane is expected to be maximized. Nevertheless, the strong hydrophilicity of the edge carboxyl groups pulls the GO sheets into bulk water, making GO behave like a regular salt dissolved in water. The GO aggregates formed at lower pH are found to be surface-active and do not exhibit the salient cmc feature associated with the formation of surfactant micelles. As a result, at pH 1 we observe a continuous reduction of surface tension (without reaching a plateau) as the GO concentration increases. The MD simulation results indicate that large GO $(C_{10}(O)_1(OH)_1)$ and GO at low pH $(C_{10}(O)_1(OH)_1(COOH)_{0.5})$ are both surface-active. Therefore, a possible way to enhance the size-sorting technique using the CO_2-floatation technique is to carry out the process at high pH such that all of the smaller GO aggregates are retained in bulk water. We hope that the study presented here provides fundamental insights into the preparation of GO or reduced GO films for electronic, optical, and biological applications by controlling their solution behavior at different pH values.

AUTHOR INFORMATION

Corresponding Author

*Author to whom all correspondence should be addressed. Email: dblank@mit.edu.

Author Contributions

§These authors contributed equally to this work.

ACKNOWLEDGMENT

C.-J.S. is grateful for partial financial support from the David H. Koch Fellowship. S.L. and D.B. are grateful for financial support from the DuPont-MIT Alliance. M.S.S. acknowledges funding from the 2009 U.S. Office of Naval Research Multi University Research Initiative (MURI) on Graphene Advanced Terahertz Engineering (GATE) at MIT, Harvard, and Boston University. M.S.S. is also grateful for a 2008 Young Investigator Program Award (YIP) from the U.S. Office of Naval Research.

REFERENCES

(1) Stankovich, S.; Dikin, D. A.; Piner, R. D.; Kohlhaas, K. A.; Kleinhammes, A.; Jia, Y.; Wu, Y.; Nguyen, S. T.; Ruoff, R. S. *Carbon* **2007**, *45*, 1558–1565.

(2) Eda, G.; Fanchini, G.; Chhowalla, M. *Nat. Nanotechnol.* **2008**, *3*, 270–274.

(3) Park, S.; Ruoff, R. S. *Nat. Nanotechnol.* **2009**, *4*, 217–224.

(4) Dreyer, D. R.; Park, S.; Bielawski, C. W.; Ruoff, R. S. *Chem. Soc. Rev.* **2010**, *39*, 228–240.

(5) Loh, K. P.; Bao, Q. L.; Eda, G.; Chhowalla, M. *Nat. Chem.* **2010**, *2*, 1015–1024.

(6) Gomez-Navarro, C.; Meyer, J. C.; Sundaram, R. S.; Chuvilin, A.; Kurasch, S.; Burghard, M.; Kern, K.; Kaiser, U. *Nano Lett.* **2010**, *10*, 1144–1148.

(7) Bagri, A.; Mattevi, C.; Acik, M.; Chabal, Y. J.; Chhowalla, M.; Shenoy, V. B. *Nat. Chem.* **2010**, *2*, 581–587.

(8) Kim, F.; Cote, L. J.; Huang, J. X. *Adv. Mater.* **2010**, *22*, 1954–1958.

(9) Lerf, A.; He, H. Y.; Forster, M.; Klinowski, J. *J. Phys. Chem. B* **1998**, *102*, 4477–4482.

(10) Li, X. L.; Zhang, G. Y.; Bai, X. D.; Sun, X. M.; Wang, X. R.; Wang, E.; Dai, H. J. *Nat. Nanotechnol.* **2008**, *3*, 538–542.

(11) Dickerson, J. H.; Hasan, S. A.; Rigueur, J. L.; Harl, R. R.; Krejci, A. J.; Gonzalo-Juan, I.; Rogers, B. R. *ACS Nano* **2010**, *4*, 7367–7372.

(12) Kim, J.; Cote, L. J.; Kim, F.; Yuan, W.; Shull, K. R.; Huang, J. X. *J. Am. Chem. Soc.* **2010**, *132*, 8180–8186.

(13) Yang, Y. F.; Song, X. H.; Liu, J. C.; Zhao, H. Y. *Langmuir* **2011**, *27*, 1186–1191.

(14) Israelachvili, J. N. *Intermolecular and Surface Forces*, 3rd ed.; Academic Press: Burlington, MA, 2011.

(15) Shenoy, V. B.; Medhekar, N. V.; Ramasubramaniam, A.; Ruoff, R. S. *ACS Nano* **2010**, *4*, 2300–2306.

(16) Hummers, W. S.; Offeman, R. E. *J. Am. Chem. Soc.* **1958**, *80*, 1339–1339.

(17) Ruoff, R. S.; Park, S.; An, J. H.; Piner, R. D.; Jung, I.; Yang, D. X.; Velamakanni, A. *Chem. Mater.* **2008**, *20*, 6592–6594.

(18) Ohshima, H. *Theory of Colloid and Interfacial Electric Phenomena*; Elsevier Academic Press: Amsterdam, 2006.

(19) Jorgensen, W. L.; Maxwell, D. S.; TiradoRives, J. *J. Am. Chem. Soc.* **1996**, *118*, 11225–11236.

(20) Van der Spoel, D.; Lindahl, E.; Hess, B.; Groenhof, G.; Mark, A. E.; Berendsen, H. J. C. *J. Comput. Chem.* **2005**, *26*, 1701–1718.

(21) Berendsen, H. J. C.; Grigera, J. R.; Straatsma, T. P. *J. Phys. Chem.* **1987**, *91*, 6269–6271.

(22) Miyamoto, S.; Kollman, P. A. *J. Comput. Chem.* **1992**, *13*, 952–962.

(23) Hess, B.; Bekker, H.; Berendsen, H. J. C.; Fraaije, J. G. E. M. *J. Comput. Chem.* **1997**, *18*, 1463–1472.

(24) Hess, B. *J. Chem. Theory Comput.* **2008**, *4*, 116–122.

(25) Shih, C. J.; Lin, S. C.; Strano, M. S.; Blankschtein, D. *J. Am. Chem. Soc.* **2010**, *132*, 14638–14648.

(26) Darden, T.; York, D.; Pedersen, L. *J. Chem. Phys.* **1993**, *98*, 10089–10092.

(27) Essmann, U.; Perera, L.; Berkowitz, M. L.; Darden, T.; Lee, H.; Pedersen, L. G. *J. Chem. Phys.* **1995**, *103*, 8577–8593.

(28) Tummala, N. R.; Striolo, A. *J. Phys. Chem. B* **2008**, *112*, 1987–2000.

(29) Patra, N.; Wang, B. Y.; Kral, P. *Nano Lett.* **2009**, *9*, 3766–3771.

(30) Hockney, R. W.; Goel, S. P.; Eastwood, J. W. *J. Comput. Phys.* **1974**, *14*, 148–158.

(31) Verlet, L. *Phys. Rev.* **1967**, *159*, 98–101.

(32) Bussi, G.; Donadio, D.; Parrinello, M. *J. Chem. Phys.* **2007**, *126*, 014101.

(33) Berendsen, H. J. C.; Postma, J. P. M; Vangunsteren, W. F.; Dinola, A.; Haak, J. R. *J. Chem. Phys.* **1984**, *81*, 3684–3690.

(34) Lin, S. C.; Shih, C. J.; Strano, M. S.; Blankschtein, D. *J. Am. Chem. Soc.* **2011**, *133*, 12810–12823.

(35) de Pablo, J. J.; Miller, C. A.; Abbott, N. L. *Langmuir* **2009**, *25*, 2811–2823.

(36) Snook, I.; Megen, W. V. *J. Chem. Phys.* **1979**, *70*, 3099–3105.

(37) Klein, J.; Kumacheva, E. *Science* **1995**, *269*, 816–819.

(38) Ren, W. C.; Zhao, J. P.; Pei, S. F.; Gao, L. B.; Cheng, H. M. *ACS Nano* **2010**, *4*, 5245–5252.

(39) Choudhury, N.; Pettitt, B. M. *J. Am. Chem. Soc.* **2005**, *127*, 3556–3567.